





Article

Annealing Temperature Effects of Seeded ZnO Thin Films on Efficiency of Photocatalytic and Photoelectrocatalytic Degradation of Tetracycline Hydrochloride in Water

Ghaida M. Wazzan ^{1,*}, Jwahr M. AlGhamdi ^{1,*}, Nuhu Dalhat Mu'azu ², Tarek Said Kayed ³, Emre Cevik ⁴ and Khaled A. Elsayed ³

¹ Department of Chemistry, College of Science, Imam Abdulrahman Bin Faisal University, P.O. Box 1982, Dammam 31451, Saudi Arabia

² Department of Environmental Engineering, College of Engineering, Imam Abdulrahman Bin Faisal University, P.O. Box 1982, Dammam 31451, Saudi Arabia; nmdalhat@iau.edu.sa

³ Department of Basic Engineering Sciences, College of Engineering, Imam Abdulrahman Bin Faisal University, P.O. Box 1982, Dammam 31451, Saudi Arabia; tkayed@iau.edu.sa (T.S.K.); kaelsayed@iau.edu.sa (K.A.E.)

⁴ Bioenergy Research Unit, Department of Biophysics, Institute for Research and Medical Consultations (IRMC), Imam Abdulrahman Bin Faisal University, P.O. Box 1982, Dammam 31441, Saudi Arabia; ecevik@iau.edu.sa

* Correspondence: 2210500175@iau.edu.sa (G.M.W.); jmalghamdi@iau.edu.sa (J.M.A.)

Abstract: In this study, seeded zinc oxide (Z-ZnO) thin films were fabricated by a two-step electrochemical deposition process. Different annealing temperatures (300, 400, 500, and 600 °C) were investigated to determine the most effective temperature for the photocatalytic activity. Comprehensive analyses were conducted using X-Ray Diffraction (XRD), scanning electron microscopy (SEM), and UV–visible spectrophotometry. The XRD results confirmed the formation of a wurtzite hexagonal structure, with the highest crystallinity observed at 400 °C. The lowest band gap value, 3.29 eV, was also recorded for Z-ZnO thin film annealed at 400 °C. SEM images revealed that the thin film treated at 400 °C exhibited a well-defined and uniform structure, contributing to its enhanced properties. The photocatalytic efficiency of ZnO (without seeding layer) and Z-ZnO thin films annealed at 400 °C was evaluated through the degradation of tetracycline hydrochloride (TCH) to prove the effect of the presence of a primary seeding layer on ZnO 400 °C thin film efficiency. The degradation efficiency of ZnO thin film without seeding layer was 69.8%. By applying a seeding layer in Z-ZnO 400 °C thin film, the degradation efficiency has been increased to 75.8%. On the other hand, Z-ZnO 400 °C thin film achieved a high degradation efficiency of 82.6% over 300 min in the photoelectrocatalytic system. The obtained Z-ZnO thin films annealed at 400 °C are highly effective photocatalysts and photoelectrocatalysts, offering a significant potential for the degradation of pharmaceuticals and other pollutants in water.

Keywords: electrochemical deposition; photocatalysis; photoelectrocatalysis; thin film; tetracycline hydrochloride; zinc oxide



Academic Editors: Francisco Javier Rivas Toledo and Jorge Bedia

Received: 27 October 2024

Revised: 1 January 2025

Accepted: 3 January 2025

Published: 14 January 2025

Citation: Wazzan, G.M.; AlGhamdi, J.M.; Mu'azu, N.D.; Kayed, T.S.; Cevik, E.; Elsayed, K.A. Annealing Temperature Effects of Seeded ZnO Thin Films on Efficiency of Photocatalytic and Photoelectrocatalytic Degradation of Tetracycline Hydrochloride in Water. *Catalysts* **2025**, *15*, 71. <https://doi.org/10.3390/catal15010071>

Copyright: © 2025 by the authors. Licensee MDPI, Basel, Switzerland. This article is an open access article distributed under the terms and conditions of the Creative Commons Attribution (CC BY) license (<https://creativecommons.org/licenses/by/4.0/>).

1. Introduction

Tetracycline hydrochloride (TCH) is a widely used antibiotic in human and veterinary medicine, agriculture, and animal feeds for livestock, cattle, and poultry due to its excellent antibacterial properties [1]. However, its presence as a pollutant in water is a growing concern. When released into aquatic ecosystems through wastewater discharge or agricultural runoff, TCH can contaminate water sources. Additionally, the overuse and improper disposal of TCH contributes to antibiotic resistance, worsening the issue [2].

Effective monitoring and proper wastewater treatment methods are essential to minimize the risk of TCH in water systems. Various methods have been studied to remove TCH from water, including biodegradation [3], and adsorption [4]. Unfortunately, TCH is difficult to completely remove from water by biological or physical treatment methods due to its high chemical stability [1].

Heterogeneous photocatalytic oxidation is an advanced, eco-friendly method for effectively removing antibiotics from water. This process utilizes suitable photocatalysts, which, when illuminated, generate reactive oxygen species such as hydroxyl radicals [5]. These radicals are capable of oxidizing and breaking down TCH molecules into simpler, less harmful byproducts [2,6–8].

Various photocatalysts have been tested for the removal of organic pollutants in water such as titanium dioxide and zinc oxide (ZnO) [9,10]. However, practical applications face challenges such as the difficulty in separating and recovering suspended photocatalysts and the high recombination rate between photogenerated electrons and holes [11]. To address these issues, researchers have explored combining photocatalysis with other processes to enhance degradation efficiency.

A notable development in this field is the integration of photocatalysis with electrochemistry, known as photoelectrocatalysis (PEC) [12]. In this combined process, the photocatalyst is immobilized on a conductive material to form a photoelectrode, with an anodic bias potential applied to the photoelectrode. This approach helps avoid catalyst loss during recovery and enhances photocatalytic efficiency by preventing nanoparticle aggregation and facilitating easier separation from the solution [13]. Despite these improvements, low anodic bias potentials have limited the effectiveness of electrochemical oxidation. Consequently, this combined process is essentially an optimized form of photocatalysis.

ZnO-based photocatalysis is widely used due to ZnO's efficiency as a semiconductor with a wide band gap of 3.37 eV, which allows it to absorb a broad range of ultraviolet (UV) and it can be modified to reach the visible light region, thus enabling various photochemical reactions [14,15]. ZnO is stable, low-cost, abundant, and environmentally friendly, making it an attractive choice for water purification [16]. However, its high recombination rate decreases photocatalytic activity [15]. To enhance efficiency, techniques such as metal–nonmetal doping [17], heterojunction formation [18], surface modification [19], dye sensitizing [20], and post-treatment methods like annealing have been developed. These methods improve light absorption, charge separation, and surface reactivity, thereby reducing electron–hole recombination and extending light absorption into the visible range [21].

Using ZnO as a slurry (powder) catalyst can lead to nanoparticle aggregation and complicate catalyst separation [22]. To mitigate this, ZnO thin films have been utilized [23]. Thin films can be easily removed from the medium after degradation without filtration and can be reused. Various methods, including sol–gel, hydrothermal, successive ionic layer adsorption and reaction, and electrochemical deposition, are used to prepare ZnO thin films [24–27]. Electrochemical deposition, or electrodeposition, is a versatile method that involves the controlled electrochemical reduction of Zn ions onto an electrode surface to form a thin ZnO film layer. This method allows precise control over film thickness, composition, and morphology [23,28,29].

Direct electrodeposition can sometimes result in a wide grain size distribution, low optical performance, and high defect concentration. To address these issues, a seeding layer has recently been employed to improve the quality and performance of ZnO films. Different methods have been discovered for seed layers, typically deposited by methods like spin coating, dip coating, or chemical bath deposition. This nucleation layer facilitates controlled growth of the ZnO film, ensuring uniformity and enhancing optical properties [30–32]. Studies have shown that the use of a ZnO seed layer not only improves the

adhesion of the deposited ZnO film but also enhanced crystallinity, increases its surface roughness, surface area, and optimized electrical properties, contributing to more efficient photocatalytic performance [31,33]. As far as the authors know, although numerous efforts for the fabrication of ZnO thin films with various preparation methods, reports on utilizing the effect of a primary seeding layer using a two-step electrochemical deposition are still limited [34].

In addition to the use of a seeding layer, another critical factor influencing the properties of ZnO thin films is the annealing process. Annealing, which involves heating the material to a specific temperature and maintaining it for a defined period, plays a significant role in optimizing the properties of ZnO films used in catalysis. Optimizing annealing conditions, including temperature, duration, and atmosphere, is crucial for tailoring the ZnO thin film's structure and performance as a catalyst photoanode [31,35,36].

Several studies have shown that annealing at temperatures around 400 °C significantly improves the structural quality of ZnO, leading to better photocatalytic performance. For example, a study demonstrated that ZnO films annealed at 400 °C exhibited superior photocatalytic activity due to enhanced crystallinity and reduced surface defects, which are known to act as recombination centers for electron–hole pairs [37]. Furthermore, annealing at higher temperatures often leads to a reduction in surface area due to grain growth, which could influence the overall photocatalytic performance depending on the balance between crystallinity and surface area [38].

To the best of our knowledge, the literature on the photocatalytic removal of TCH from water is limited, particularly concerning methods with low removal efficiency [39]. Enhancing removal efficiency often requires increasing the concentration of the photocatalyst [40]. However, this approach complicates the separation of the catalyst from the treated medium and increases material costs, resulting in more challenging and costly operational procedures [41]. Moreover, the photocatalytic performance of pure ZnO for TCH degradation is often limited by its rapid electron–hole recombination and lack of visible-light activity [42].

In summary, the photocatalytic degradation of tetracycline hydrochloride is a rapidly evolving area of research, with various strategies being employed to enhance the efficiency of photocatalysts. However, further research is needed to improve their practical application.

Despite the significant progress in photocatalysis, the area of PEC for TCH removal remains relatively underexplored [43]. PEC combines the advantages of photocatalysis with electrochemical assistance, where an external potential is applied to the photocatalyst to improve charge separation, enhance electron transport, and extend the photocatalytic reaction duration [44]. This approach has shown promise in improving the degradation efficiency of organic pollutants in general, most current PEC studies for water treatment have focused on pollutants such as dyes [45], phenolic compounds [46], and other pharmaceuticals [47], with TCH receiving far less attention [48].

In conclusion, the research on PEC for TCH degradation is still in its infancy. This indicates a strong need for further investigation into the PEC approach for efficient and sustainable TCH removal from water.

To close this gap in research and advance the field of water treatment, this study introduces a novel approach by combining a two-step electrochemical deposition method for fabricating ZnO thin films with a low catalyst concentration, optimized annealing conditions, and the incorporation of a seeding layer. This research aims to enhance the photocatalytic and photoelectrocatalytic performance of ZnO thin films, specifically targeting the degradation of TCH from water. The novelty of this work lies in the systematic explo-

ration of these factors to improve the efficiency of TCH removal, making it a promising strategy for future sustainable water treatment technologies.

2. Results and Discussion

2.1. XRD Analysis for Z-ZnO Thin Films

X-Ray Diffraction (XRD) analysis was utilized to validate the presence of the hexagonal wurtzite phase in Z-ZnO thin films grown through the electrochemical deposition method. These films were fabricated by maintaining a constant temperature of 80 °C on a fluorine-doped tin oxide glass (FTO) substrate. Furthermore, XRD patterns were employed to investigate how variations in annealing temperature affected the crystal structure of the Z-ZnO thin films.

In Figure 1, all diffraction peaks were identified for Z-ZnO films electrodeposited on FTO glass for different annealing temperatures ranging from 300 to 600 °C. Distinct peaks were attributed to the FTO glass substrate marked with a star (*) based on the reference (JCPDS No. 77-0447). According to the literature, it was observed that the films exhibited superior crystallinity when deposited at 80 °C, as indicated by the presence of high-intensity, sharp diffraction peaks [49]. The primary ZnO peaks were centered at 2θ angles of 31.8°, 34.4°, and 36.3°, corresponding to the (100), (002), and (101) crystal planes, respectively. The lattice planes and peak positions of our prepared Z-ZnO thin films closely matched those of reference patterns for ZnO (JCPDS No. 00-036-1451), affirming the successful development of ZnO in the hexagonal wurtzite phase [50]. Peaks corresponding to Zinc Hydroxide ($\text{Zn}(\text{OH})_2$) marked with (•), matching the reference (JCPDS card no. 38-0385) were observed in the XRD patterns at low annealing temperatures, which decompose into ZnO at higher temperatures, explaining their disappearance at higher annealing temperatures [51].

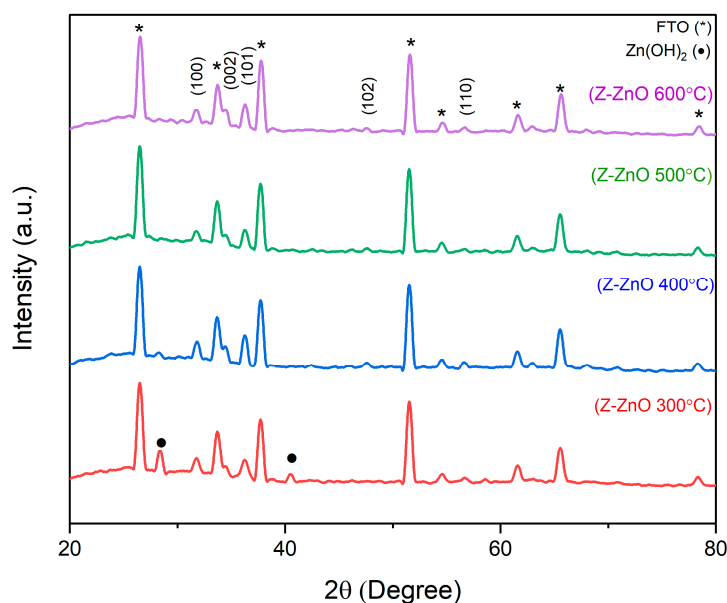


Figure 1. XRD spectrum for Z-ZnO 300 °C, Z-ZnO 400 °C, Z-ZnO 500 °C, and Z-ZnO 600 °C thin film samples.

The intensity of the diffraction peaks for ZnO was found to be highly dependent on the annealing temperature. As the annealing temperature increases to 400 °C, the XRD peak intensity increases. This is because higher temperatures can help improve crystallinity and reduce defects in the thin film [51,52]. The sharper and more intense peaks in the XRD pattern indicate a more ordered and crystalline structure.

It is important to note that there is an optimal annealing temperature range for achieving the desired XRD peak intensity and crystal size, and the best results have been achieved with annealing at 400 °C. Exceeding this range might lead to the growth of excessive defects or even the degradation of the film's properties. As observed with 500 °C and 600 °C, the XRD peak intensity decreased compared to the sample annealed at 400 °C, although the ZnO hexagonal structure remained intact [53].

The reduction in peak intensity at 500 °C can be attributed to several factors. At higher temperatures, excessive grain growth, leads to an increase in particle size, which in turn causes imperfections within the crystal structure. These structural imperfections cause the X-rays to scatter more widely, leading to a decrease in the overall intensity of the diffraction peaks. Additionally, prolonged exposure to high temperatures around 600 °C can induce thermal stress within the thin film, potentially resulting in microcracks or other structural defects that negatively affect the crystalline quality of the material [37].

So, it is crucial to conduct controlled experiments to determine the best annealing conditions for ZnO thin film.

Moreover, XRD data were utilized to calculate the average grain size using Scherrer's Equation (1):

$$D = \frac{k\lambda}{\beta \cos\theta} \quad (1)$$

which considers parameters such as crystallite size (D), Scherrer's constant (k), wavelength of the X-ray source (λ), (β) is the full width at half maximum intensity (FWHM), and Bragg's diffraction angle (θ).

The strongest ZnO peak observed at 2θ around 36.3, corresponding to the (101) crystal plane, had FWHM values of 0.2450, 0.3267, 0.2450, and 0.2450 for Z-ZnO at 300 °C, Z-ZnO at 400 °C, Z-ZnO at 500 °C, and Z-ZnO at 600 °C, respectively.

Applying Scherrer's equation to the FWHM values of the (101) peak line allowed the calculation of the average crystallite size for Z-ZnO 300 °C, Z-ZnO 400 °C, Z-ZnO 500 °C, and Z-ZnO 600 °C, in that order; the crystals size were 34.13 nm, 25.6 nm, 34.13 nm, and 34.12 nm, respectively. The grain size of the prepared ZnO thin films increased with higher annealing temperatures, aligning with prior research on the impact of annealing on the crystallinity of ZnO thin films [54].

2.2. UV-Vis Absorption Spectra

UV-VIS absorption spectra were employed to analyze the optical absorption characteristics and the band gap of the film material. It is well-known that the optical properties of transparent conductive films are predominantly influenced by the deposition techniques and the specific preparation conditions used during film fabrication [55].

Figure 2 displays the UV-Vis absorption spectra of prepared ZnO thin films subjected to various annealing temperatures, ranging from 300 °C to 600 °C.

As depicted in Figure 2a, the spectra were recorded across the wavelength range of 250 to 600 nm. Notably, Z-ZnO 300 °C, Z-ZnO 400 °C, Z-ZnO 500 °C, and Z-ZnO 600 °C thin films exhibited distinct absorption peaks at λ_{\max} values of 355 nm, 372 nm, 371 nm, and 369 nm, respectively.

To assess the optical band gap of the film material, Tauc plots were generated and are presented in Figure 2b. Tauc equation was employed to calculate the band gap of the samples in Equation (2).

$$(\alpha h \nu)^2 = A (h \nu - E_g) \quad (2)$$

where α is the absorption coefficient (cm^{-1}) being a function of wavelength $\alpha(\lambda)$, h is Planck constant (Js), ν is frequency (Hz), E_g is an optical band gap of a semiconductor (eV), A is proportionality constant [56].

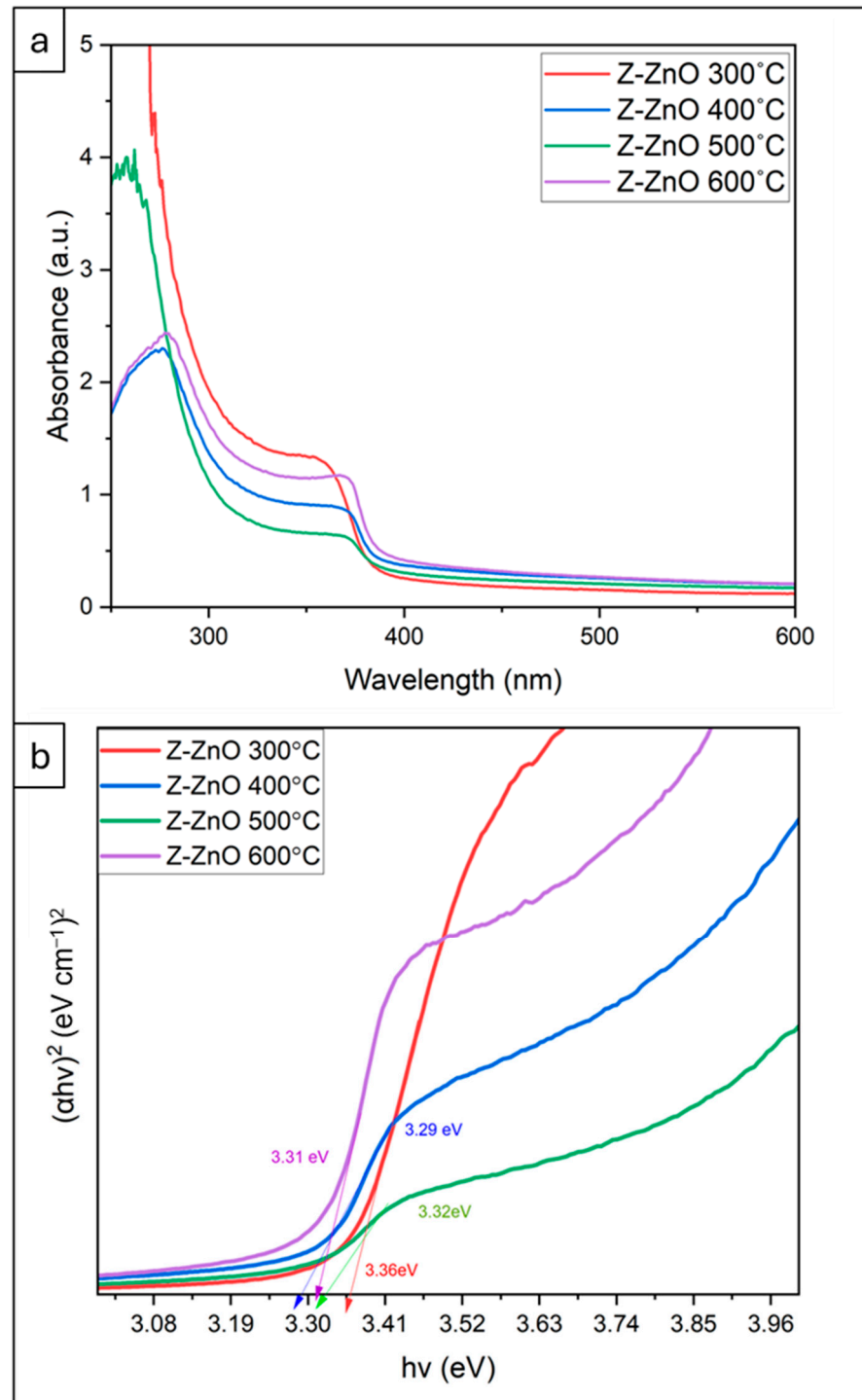


Figure 2. UV-Vis absorption spectra for the optical properties. (a) UV-VIS absorption spectra for Z-ZnO 300 °C, Z-ZnO 400 °C, Z-ZnO 500 °C, Z-ZnO 600 °C thin films and (b) TAUC plot between $(\alpha h\nu)^2$ and $h\nu$ to calculate the band gap for Z-ZnO 300 °C, Z-ZnO 400 °C, Z-ZnO 500 °C, Z-ZnO 600 °C thin films.

The energy gap of the samples was determined by plotting $(\alpha h\nu)^2$ against the photon energy ($h\nu$) according to the Tauc relationship. The calculated band gap values for the prepared thin films were 3.36 eV, 3.29 eV, 3.32 eV, and 3.31 eV for Z-ZnO 300 °C, Z-ZnO 400 °C, Z-ZnO 500 °C, and Z-ZnO 600 °C thin films, respectively, as presented in Figure 2.

The best results for Z-ZnO film are achieved with an annealing temperature of 400 °C which results in a modest reduction in the band gap; this reduction in the bandgap can be attributed to a reduction in structural defects, such as oxygen vacancies and grain

boundaries, which are common in as-deposited films. Higher annealing temperatures help to reduce these defects, particularly oxygen vacancies, which lowers the carrier concentration in the conduction band [57]. Additionally, the annealing process improves crystallinity, reducing the number of defects and relieving strain within the films. These improvements in crystallinity and structural order contribute to the observed decrease in the bandgap energy, enhancing the generation of electron–hole pairs, thereby improving the material’s photocatalytic and optical properties [58–60].

2.3. SEM Analysis

The morphology, crystal structure and grain size of the thin films were assessed through scanning electron microscopy (SEM). Figure 3 presents SEM images illustrating the effects of annealing temperatures. All the coated samples obtained an average thickness of $10 \pm 1 \mu\text{m}$. Annealing at a relatively low temperature of $300\text{ }^\circ\text{C}$ resulted in the formation of large particles lacking a discernible crystal structure in the Z-ZnO thin film. Raising the annealing temperature to $400\text{ }^\circ\text{C}$, in conjunction with the presence of a primary seeding layer, promoted crystallization and enhanced the crystal quality of the ZnO thin films. The grains can be calculated from the SEM image to be approximately in average to be 500 nm in size; these grains displayed a distinct hexagonal shape with a random distribution, and the particle size was notably smaller compared to the film annealed at $300\text{ }^\circ\text{C}$, leading to a highly increased surface area [61,62].

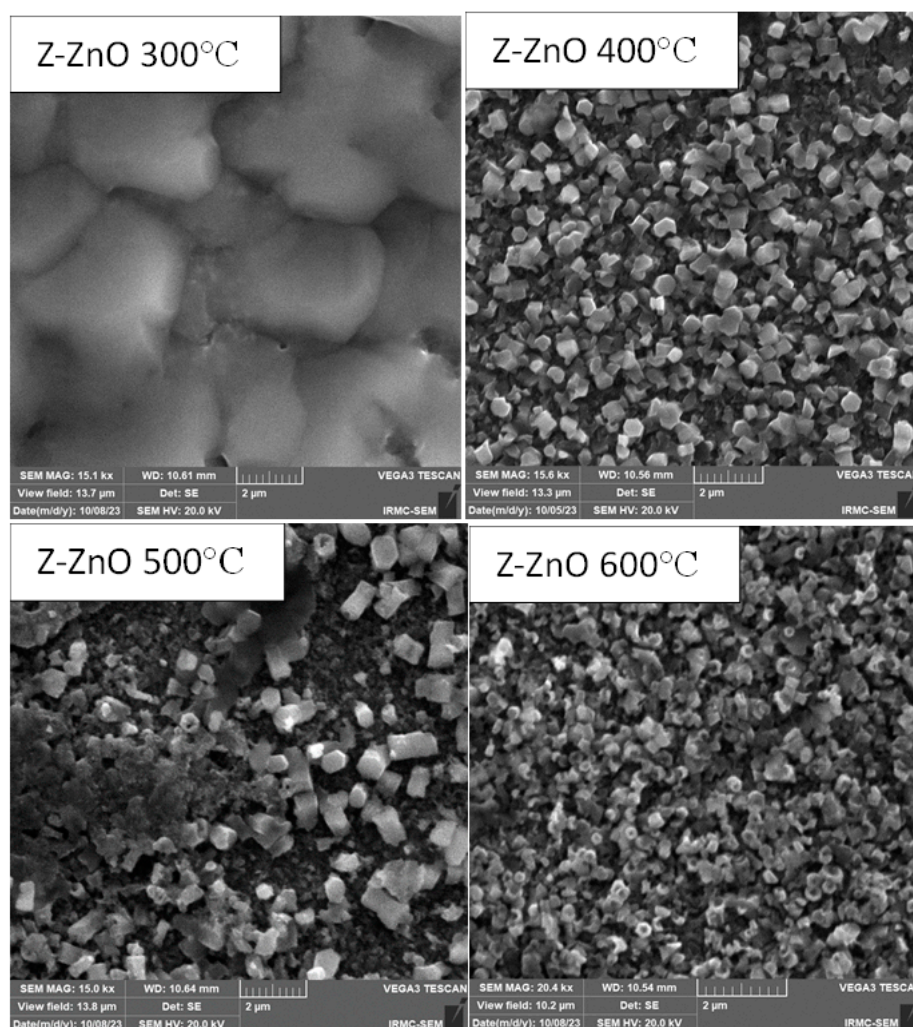


Figure 3. SEM characterization for Z-ZnO thin film comparing different annealing temperatures (300, 400, 500, 600 °C).

Further elevating the annealing temperature to 500 °C induced grain growth, around 700 nm, causing a reduction in specific surface area and an increase in particle size due to the aggregation and agglomeration of ZnO particles. However, exceedingly high annealing temperatures of 600 °C resulted in smaller grain size appearing to decrease to about 250 nm with fragile, broken, and shattered grains, some of which exhibited a hexagonal structure with a hollowed-out center.

These results are consistent with the previous literature, where a study investigating annealing temperatures ranging from 350 to 500 °C for aluminum-doped zinc oxide thin films reported that both the grain size and the overall crystalline quality of the films improved as the annealing temperature increased, up to an optimal point [54].

In summary, based on SEM characterization comparing different annealing temperatures (300, 400, 500, 600 °C), the most favorable morphological orientation for Z-ZnO particles was achieved at an annealing temperature of 400 °C, aligning with UV-VIS absorption and band gap findings. Additionally, the XRD analysis showed that the smallest crystallite size, which is related to the size of the coherent regions within a grain, was attained at the same annealing temperature of 400 °C. Furthermore, the SEM data reveal higher average grain size values compared to the crystallite size obtained from XRD measurements using the Scherrer equation. This difference, commonly observed in other thin films [63], occurs because the grain size measured in SEM reflects the surface morphology of grains, which are composed of multiple crystallites, resulting in larger grain size values.

2.4. Photocatalytic Performance

2.4.1. Effect of Annealing Temperature

Annealing plays a crucial role in the preparation of thin films, particularly in determining the optimal temperature for achieving high photocatalytic activity in ZnO thin films. The choice of annealing temperature significantly affects the crystal structure, morphology, and electronic properties of the thin film, thereby impacting its photocatalytic performance [64]. Generally, higher annealing temperatures promote crystallization and improve the quality of ZnO thin films, leading to enhanced charge transport properties and increased photocatalytic activity. The annealing process helps eliminate defects such as oxygen vacancies and interstitials, which can act as recombination centers for photo-induced charge carriers. This reduction in defect density improves the separation and mobility of electrons and holes, facilitating efficient charge transfer to the electrode–electrolyte interface. However, excessively high annealing temperatures can result in grain growth, reducing the specific surface area and potentially limiting the availability of active sites for photocatalytic reactions. Therefore, selecting an optimal annealing temperature is crucial to balance crystal quality, defect density, and surface area, maximizing the photocatalytic activity of ZnO thin films [35,36,65].

In Figure 4a, four different annealing temperatures (300, 400, 500, 600 °C) were tested on Z-ZnO thin films to determine the temperature that exhibits the best photocatalytic activity for the degradation of TCH in water. All the experiments were carried out in three (3) replicated runs. Accordingly, for Z-ZnO 300 °C, Z-ZnO 400 °C, Z-ZnO 500 °C, Z-ZnO 600 °C and ZnO 400 °C the calculated standard deviation (SD) was 0.03, 0.02, 0.03, 0.002 and 0.25 while the standard error of estimate (SE) was 0.02, 0.01, 0.02, 0.001, and 0.14 with mean TCH removal of 73.02%, 75.84%, 74.23%, 74.03, and 69.6%, respectively. These low values of the SD and SE confirm the experimental results reproducibility as well as consistency of different modes of trials. The mean values for the TCH removal are reported for all the experimental runs throughout the manuscript. Figure 4a shows that the highest degradation efficiency of 75.85% was achieved at an annealing temperature of 400 °C over a 5 h reaction period, while the lowest annealing temperature resulted in

a minimum degradation efficiency of 73%. Increasing the annealing temperature beyond 400 °C led to a decrease in efficiency.

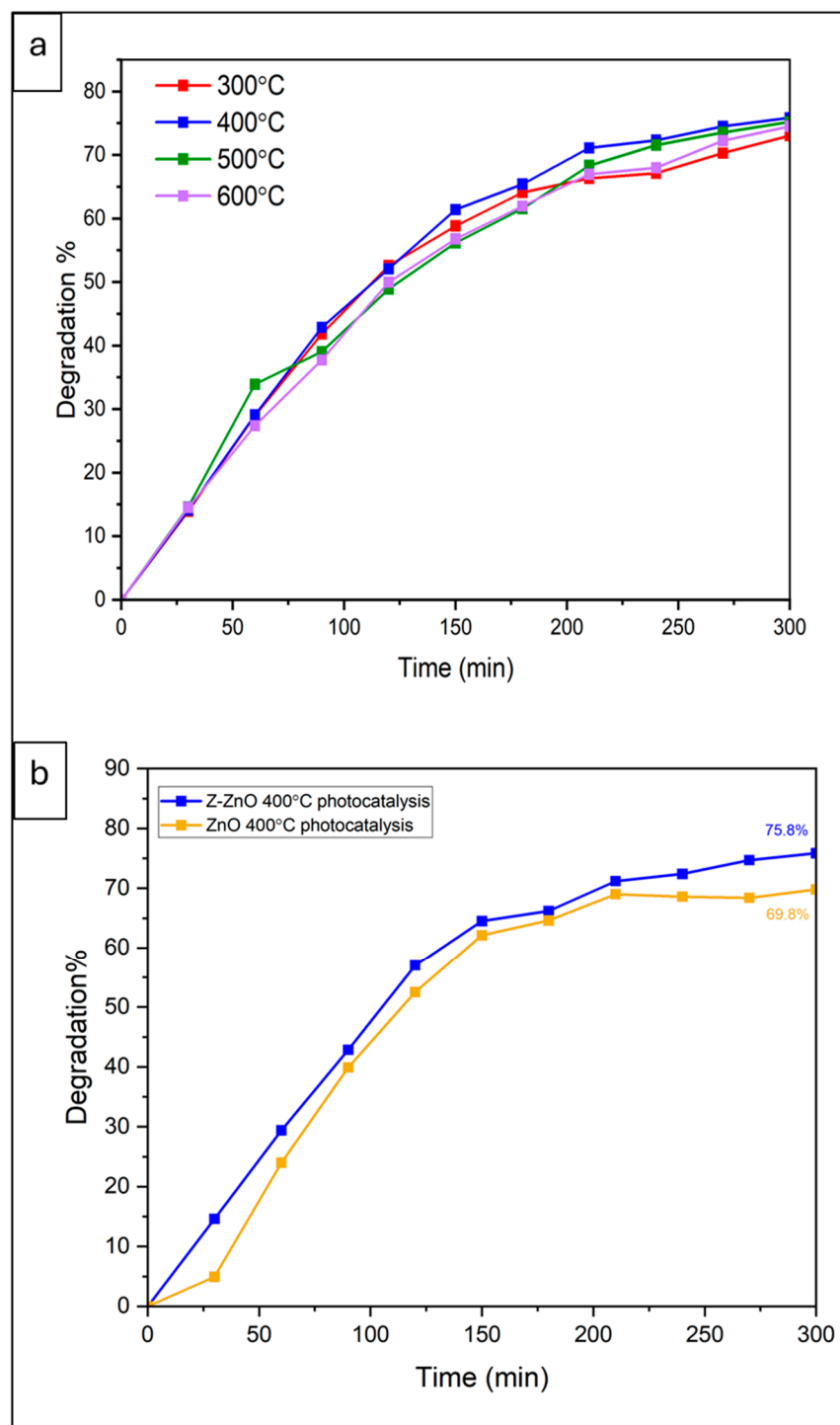


Figure 4. (a) Effect of different annealing temperatures (300, 400, 500, 600 °C) of Z-ZnO on the photocatalytic degradation of 30 ppm TCH under UV light for 300 min. (b) Effect of seeding layer on ZnO thin film for the photocatalytic degradation of 30 ppm TCH under UV light for 300 min.

This result is consistent with the characterization findings, band gap calculations, and the literature review. However, it appears to contrast with the findings of a study investigating the effect of annealing temperatures (ranging from 0 to 800 °C) on ZnO thin films prepared by radio frequency sputtering. The authors of that study demonstrated that annealing temperatures above 400 °C led to a systematic increase in band gap values. This

increase in band gap energy suggests a reduction in defects and vacancies within the ZnO films [36].

2.4.2. Effect of Seeding Layer

The impact of a seeding layer, applied before the deposition of ZnO, was investigated. The seeding layer was created through electrodeposition by exposing the FTO glass substrate to a concentrated Zinc solution for a short duration of 30 S. The photocatalytic efficiency of the films prepared with and without the seeding layer was compared in a photocatalytic system. The system utilized a 395 nm lamp as the light source and a 30 ppm TCH solution. The photocatalytic degradation efficiency was evaluated over a 300 min reaction period as shown in Figure 4b.

The results demonstrated an improvement in the photocatalytic efficiency of Z-ZnO thin films compared to ZnO thin films without a seeding layer. This enhancement can be attributed to modifications in surface properties, such as crystal structure and morphology, as well as improved adhesion of the ZnO film to the FTO substrate. These factors contribute to the stability and recyclability of thin film [66,67].

This result appears to contradict the findings of López Guemez et al. on the hydrothermal growth of ZnO nanorods and nanoflowers on a seeding layer deposited via spin coating. The study concluded that the presence of a seeding layer on ZnO thin films significantly enhances the photocatalytic degradation of methylene blue. Their experiments achieved 100% dye degradation in 120 min using the prepared thin film with a seeding layer, and they demonstrated that the thin film exhibited excellent reusability over five consecutive cycles, attributed to improved adhesion [66].

2.5. Comparison Between Photocatalytic and Photoelectrocatalytic Performance

Figure 5 illustrates the degradation percentage versus time for Z-ZnO 400 °C thin film (in the dark), photolysis, photocatalysis, and photoelectrocatalysis.

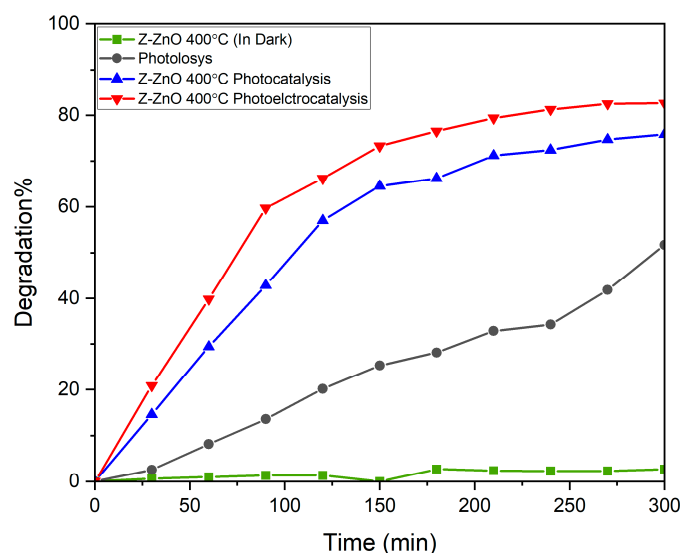


Figure 5. The degradation of 30 ppm TCH under UV light for 300 min using Z-ZnO 400 °C thin film (in the dark), photolysis, photocatalysis, and photoelectrocatalysis methods.

To fully understand the effects of different removal methods, a comparison between these methods should be made to evaluate their relative efficiencies.

The study investigated the removal of TCH using various degradation methods with Z-ZnO 400 °C thin films. All the removal methods were compared to assess their efficiency

in removing TCH from a 100 mL solution containing 30 ppm TCH and 0.1 M Na₂SO₄, with a reaction time of 300 min.

Controlled experiments were initially conducted to assess the adsorption capacity of the Z-ZnO 400 °C film (in the dark) and the degradation potential of the light source. The adsorption by Z-ZnO 400 °C resulted in less than 2.5% removal of TCH, which was attributed to the lack of electron excitation and the absence of reactive species generation, suggesting that tetracycline adsorption had a negligible effect on its elimination. In contrast, photolysis resulted in a 51% degradation of TCH, with tetracycline degrading rapidly under irradiation. This indicates that the degradation process was significantly enhanced by the light source. These findings are consistent with previous studies on TCH degradation [68].

However, when the same Z-ZnO 400 °C film was used in a photocatalysis system, where both light and the material's catalytic properties were engaged, a significantly higher degradation efficiency of 75.85% was achieved. In an even more advanced system, the PEC process, where both light and an external electric field were applied, the degradation efficiency further increased to 82.6%.

This enhancement is due to the synergistic effects of light-induced generation of reactive oxygen species and the external electric field. The photocatalysis method relies solely on light to excite the electrons and generate reactive species, whereas the PEC method benefits from additional electron excitation and enhanced charge separation facilitated by the electric field. This combined approach significantly improves the degradation efficiency of TCH by accelerating the generation of reactive species and enhancing their interaction with the pollutant. All experimental runs were carried out in three (3) replicates. Accordingly, for the experiments in dark, photolysis, Z-ZnO 400 photocatalysis and Z-ZnO 400 photo-electrocatalysis the calculated standard deviation (SD) was 0.06, 0.42, 0.02 and 0.17, while the standard error of estimate (SE) was 0.03, 0.3, 0.01 and 0.1 with mean TCH removal of 2.7%, 52%, 75.84% and 82.5%, respectively. These low values of the SD and SE confirm the experimental results reproducibility as well as the consistency of different modes of trials. The mean values for the TCH removal are reported for all the experimental runs throughout the manuscript.

This result matches with the literature, as there are various researchers who have highlighted the superior performance of photoelectrocatalytic systems compared to conventional photocatalysis due to the synergy between the light-induced electron excitation and the applied electric field.

For instance, a study investigated the PEC degradation of rhodamine B using a ZnO photoanode prepared by a two-step electrodeposition under UV light and an applied external potential. The study compared the photolysis, photocatalytic, electrocatalytic, and photo-electrocatalytic performances of the ZnO films. The study demonstrated that the degradation efficiency of RhB using PEC process exhibited significantly enhanced higher efficiency from 20% in photocatalysis to 100% in PEC. This improvement was attributed to the effective separation of electron–hole pairs facilitated by the electric field, which prevented recombination and enhanced the production of reactive oxygen species in the interface of ZnO photoanode. This result clearly illustrates the significant synergistic effect of PEC for the degradation of the pollutant which is higher than the photocatalysis process alone [69].

Moreover, a comparative study compared the PEC degradation of glucose using TiO₂ films and highlighted that PEC systems consistently outperformed photocatalysis. The overall oxidation efficiency of the PEC process was better than the photocatalysis process. The researchers concluded that the external electric field played a crucial role in enhancing electron–hole separation, extending the lifetime of reactive species, and ensuring higher pollutant degradation [70].

Based on these findings, we have observed an improvement in degradation efficiency using the PEC system compared to traditional photocatalysis. However, there remains potential for further research to explore additional factors and enhance the degradation rate for TCH pollutant, positioning this technology as a promising future solution for sustainable water treatment. Consequently, additional studies will be conducted to optimize the performance of ZnO and achieve complete degradation within a shorter timeframe.

3. Materials and Methods

3.1. Materials

The chemicals utilized in this study are as follows: fluorine-doped tin oxide (FTO) from SOLARONIX (Aubonne, VD, Switzerland), zinc chloride (ZnCl_2) from Schalau (Vöhringen, Bavaria, Germany), potassium chloride (KCl) from LOBA Chemie (Mumbai, Maharashtra, India), Isopropanol from Honeywell (Morris Plains, NJ, USA), tetracycline hydrochloride (TCH) as a pharmaceutical pollutant from Sigma-Aldrich (St. Louis, MO, USA), sodium sulfate (Na_2SO_4) from CHEM-IMPEX (Wood Dale, IL, USA). All solutions were prepared using deionized (DI) water as a solvent; all the chemicals were analytically graded and utilized as received without any further purification.

3.2. Pretreatment of FTO Glass

A 2.2 mm thick FTO glass substrate with a resistivity of $7 \Omega/\text{sq}$ at room temperature was used. The substrate was cut into 2.5 cm^2 pieces and cleaned using isopropanol, followed by ultrasonication for 5 min. After the ultrasonication, the substrate was rinsed with deionized water three times. Finally, the substrate was dried on a hot plate for 10 min. The schematic diagram of the pretreatment setup is shown in Figure 6.



Figure 6. Scheme diagram for FTO glass pretreatment.

3.3. Seeding Layer and Electrodeposition of ZnO Layer

All electrochemical experiments were performed using a potentiostat from GAMRY instruments, (Reference 3000, Warminster, PA, USA). In a three-electrode system with the FTO glass substrate as the working electrode (cathode), a platinum sheet $0.5 \times 0.5 \text{ cm}$ served as the counter electrode (anode), and an Ag/AgCl electrode from GAMRY as the reference electrode. All the spaces between the electrodes were fixed using an electrochemical cell Teflon cover with three electrode holes. To control the electrodeposition temperature, a hot water bath with a setting temperature of $80 \text{ }^\circ\text{C}$ was used as reported in the literature [71].

Electrodeposition was carried out potentiostatically and from the resulting cyclic voltammogram, the range of possible potentials for ZnO deposition was determined and maintained at -0.9 V .

The duration of electrodeposition for the seeding layer was 30 s layer, while it was 120 min for the zinc oxide layer.

The electrodeposited layer is strongly dependent on the seeding layer, and the electrochemical growth of the seeding layer will enhance the formation of ZnO nanorods and improve the film properties. For the seeding layer, a solution of 60 mL of a high concentra-

tion ZnCl_2 5.0 mol/L and 1.0 mol/L KCl was employed. After the seeding layer, the film was dried for 10 min on a hot plate at 80°C .

The electrodeposition of ZnO thin film layer was performed by a solution of 60 mL of 5.0 mmol/L ZnCl_2 as a zinc precursor and 1.0 mol/L KCl as a supporting electrolyte to enhance electrical conductivity was used. After completing the electrodeposition layer, the thin film was removed from the cell, immersed in DI water to wash and remove any residue, and finally, the film was dried and annealed in an oven at different temperatures for 40 min. The schematic diagram of the experiment setup is shown in Figure 7a for the seeding layer denoted with (Z) and Figure 7b for the zinc oxide layer denoted with ZnO, therefore the samples will be denoted from now on as Z-ZnO.

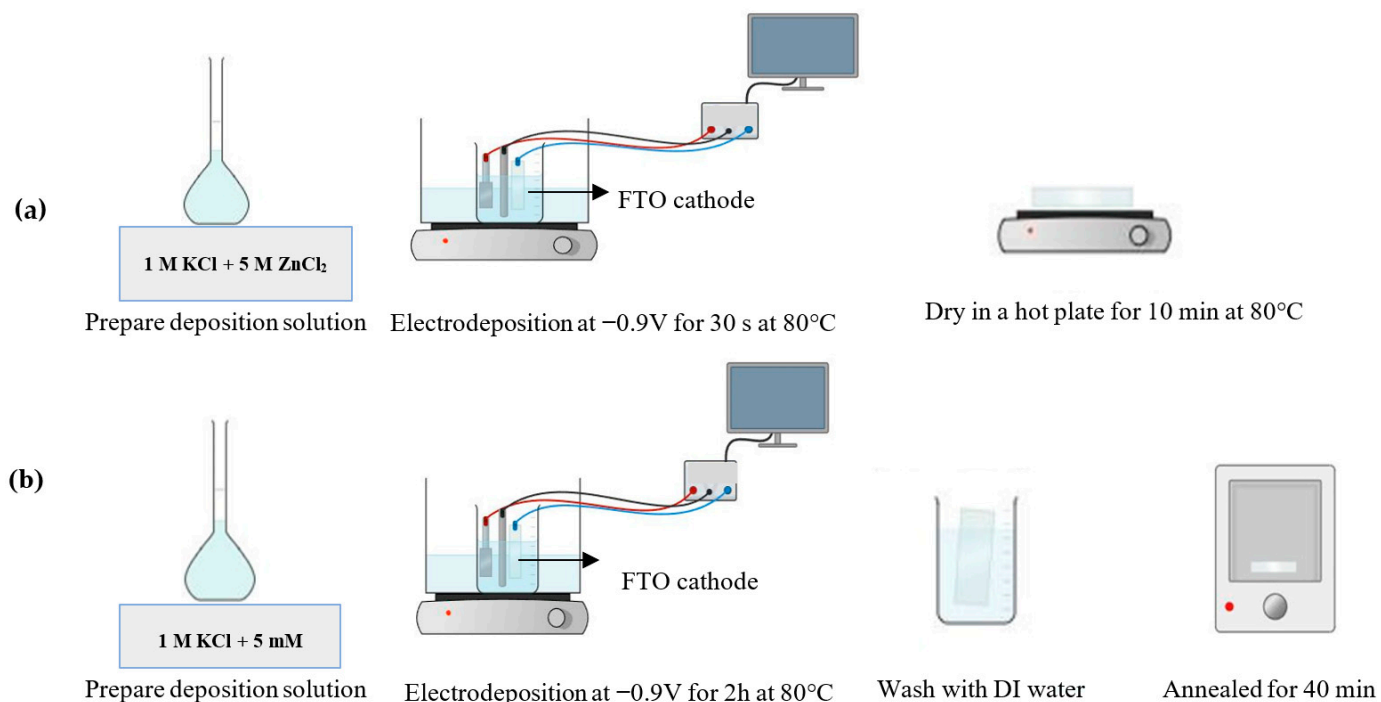


Figure 7. Scheme diagram for ZnO thin film preparation method. (a) Seeding layer (Z); (b) electrodeposition of ZnO layer.

3.4. Photocatalysis Performance

TCH was used as a pharmaceutical pollutant to evaluate the photocatalytic activity of ZnO thin films under UV light irradiation at room temperature. In a handmade photocatalyst set-up system using a 100 mL beaker made of quartz glass, a (100 W) UV lamp was used at ($\lambda = 395$ nm) as a UV source from VUSUM (Mainland China), and placed under the beaker to make sure that the full light was exposed to the solution. Also, The FTO catalyst film was placed inside the beaker. All setups were kept in a box covered with aluminum foil to prevent UV light exposure. The absorption peak of TCH at ($\lambda_{\text{max}} = 360$ nm) is employed to examine the photocatalytic degradation for TCH. For each photocatalytic test, the catalyst film was set inside a 100 mL solution of 30 ppm TCH. The solution was exposed to UV light under room temperature. Every 30 min, 3 mL of the solution was collected in a cuvette without centrifuging and evaluated using a UV-VIS spectrophotometer HACH, DR6000 (Loveland, CO, USA), to obtain the concentration and absorbance of the pollutant in the sample.

The percentage of pollutant degradation was calculated using Equation (3):

$$\text{Degradation percent} = \frac{A_0 - A_t}{A_0} \times 100 \quad (3)$$

where A_0 is the initial absorbance of the pollutant before the UV irradiation and A_t is the absorbance of the sample taken in a certain time.

3.5. Photoelectrocatalysis Performance

The performance of the prepared catalysts in photo-electrocatalysis system was investigated using a custom-made photo-electrocatalyst setup connected to a Potentiostat with a three-electrode system. The setup included an Ag/AgCl electrode as a reference electrode, a platinum sheet as the working electrode (cathode), and the catalyst film as the counter electrode (anode). A quartz glass beaker with a Teflon cover was used to house the electrodes and the catalyst thin film. The beaker was illuminated with a 100 W UV lamp emitting light at a wavelength of 395 nm. A 100 mL solution containing 30 ppm TCH as a model pharmaceutical water pollutant and 0.1 M Na_2SO_4 as a supporting electrolyte was used to evaluate the photo-electrocatalytic activity of the thin film.

Cyclic voltammetry measurements were performed with a potential range of 0 V to 2 V, and an oxidation peak was observed. The applied potential was fixed at 1.5 V. The photo-electrocatalysis reaction was initiated by applying a positive potential of 1.5 V, and the solution was exposed to UV light at room temperature. The PEC setups were placed in a box covered with aluminum foil to prevent UV light exposure as in Figure 8. The absorption peak of TCH at a wavelength of 360 nm was used to examine the photo-electrocatalytic degradation.

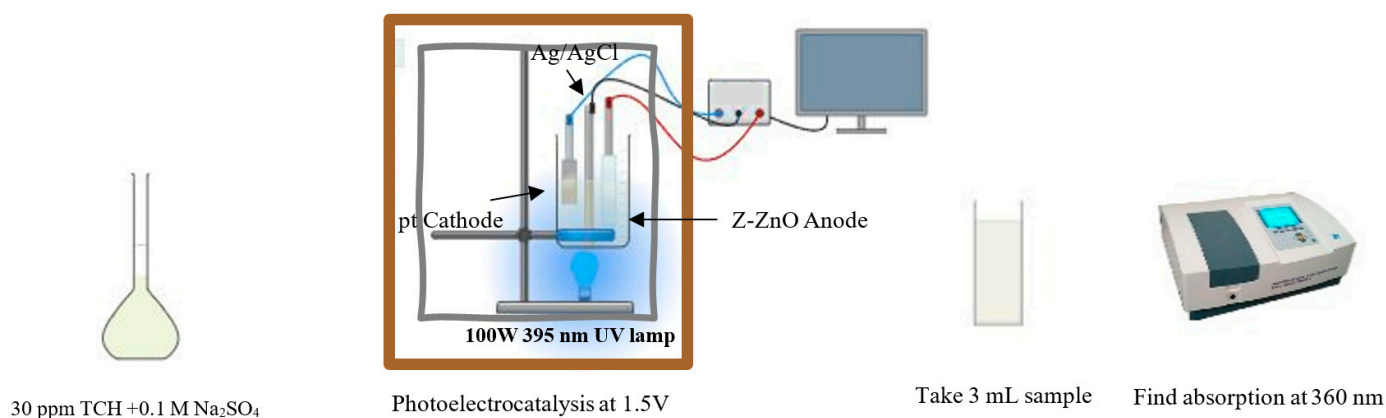


Figure 8. The photoelectrochemical reactor setups.

At specific time intervals, a 3 mL sample of the solution was collected without centrifugation and analyzed using a UV-VIS spectrophotometer HACH, DR6000 (Loveland, CO, USA), to determine the absorbance of the pollutant in the sample. The percentage of pollutant degradation was calculated using Equation (3), as previously described.

3.6. Characterization of Z-ZnO

XRD measurements were achieved using Rigaku Ultima IV X-ray diffractometer running at 40 mA and 40 kV with $\text{CuK}\alpha$ radiation ($\lambda = 1.5406 \text{ \AA}$) and a scan step size of 0.02 at a speed of $2^\circ/\text{min}$ in a range of $20\text{--}80^\circ$ at room temperature. The optical properties and the band gap were characterized by a UV-Visible spectrophotometer, UV-vis solidspec 3700. The surface morphology Z-ZnO thin films with different annealing temperatures (300, 400, 500, 600 $^\circ\text{C}$), was investigated using SEM, TESCAN VEGA3. All electrochemical measurements were performed using a potentiostat from GAMARY instruments, Reference 3000., in a three-electrode system.

4. Conclusions

In this study, ZnO thin films were successfully fabricated using a two-step electrochemical deposition process, followed by an annealing treatment at various temperatures. Comprehensive analyses confirmed the formation of ZnO in a pure hexagonal wurtzite crystal phase, with the optimal annealing temperature identified as 400 °C. With a band gap of (3.29 eV), these optimized thin films were employed for the photocatalytic degradation of TCH, a commonly found antibiotic contaminant in water. The results demonstrated that annealing the Z-ZnO thin films at 400 °C significantly enhanced their photocatalytic activity by increasing surface area, improving electron transport, and reducing electron–hole recombination. To further improve the degradation efficiency, the thin films were also tested in a photoelectrocatalytic system. This system effectively extended the lifetime of the photogenerated holes, further reducing electron–hole recombination, and consequently increasing the degradation efficiency of TCH to reach 82.6%. These findings highlight the potential of the electrodeposited Z-ZnO thin films annealed at 400 °C as highly efficient, eco-friendly catalysts for water purification. The enhanced performance of these thin films offers a promising approach to mitigating antibiotic contamination in aquatic environments, contributing to the development of sustainable water treatment technologies.

Author Contributions: G.M.W. carried out all the synthesis, film deposition, device fabrication, and characterization. J.M.A. supervised the overall project, N.D.M. advised the overall project. All authors wrote the manuscript, discussed the results, and approved the submission. G.M.W.: Writing—original draft, Software, Investigation, Formal analysis, Data curation, Methodology. J.M.A.: Writing—original draft, Writing—review and editing, Validation, Supervision. N.D.M.: Writing—original draft, Writing—review and editing, Validation, Supervision. K.A.E.: Writing—original draft, Writing—review and editing. T.S.K.: Writing—original draft. E.C.: Writing—original draft. All authors have read and agreed to the published version of the manuscript.

Funding: This research received no external funding.

Data Availability Statement: This work is ongoing as we prepare additional publications. However, any data related to this study will be made available upon request.

Acknowledgments: This work has been conducted at Imam Abdulrahman bin Faisal University using the resources of the university.

Conflicts of Interest: The authors declare that there is no conflicts of interests or personal relationships that could have appeared to influence the work reported in this paper.

References

1. Xiao, H.; Wang, Y.; Peng, H.; Zhu, Y.; Fang, D.; Wu, G.; Li, L.; Zeng, Z. Highly Efficient Degradation of Tetracycline Hydrochloride in Water by Oxygenation of Carboxymethyl Cellulose-Stabilized FeS Nanofluids. *Int. J. Environ. Res. Public Health* **2022**, *19*, 11447. [[CrossRef](#)]
2. Fang, Z.; Jiang, H.; Gong, J.; Zhang, H.; Hu, X.; Ouyang, K.; Guo, Y.; Hu, X.; Wang, H.; Wang, P. Removal of Tetracycline Hydrochloride from Water by Visible-Light Photocatalysis Using BiFeO₃/BC Materials. *Catalysts* **2022**, *12*, 1461. [[CrossRef](#)]
3. Hain, E.; Adejumo, H.; Anger, B.; Orenstein, J.; Blaney, L. Advances in Antimicrobial Activity Analysis of Fluoroquinolone, Macrolide, Sulfonamide, and Tetracycline Antibiotics for Environmental Applications through Improved Bacteria Selection. *J. Hazard. Mater.* **2021**, *415*, 125686. [[CrossRef](#)]
4. Wang, K.; Wu, J.; Zhu, M.; Zheng, Y.Z.; Tao, X. Highly Effective PH-Universal Removal of Tetracycline Hydrochloride Antibiotics by UiO-66-(COOH)₂/GO Metal–Organic Framework Composites. *J. Solid State Chem.* **2020**, *284*, 121200. [[CrossRef](#)]
5. Byrne, C.; Subramanian, G.; Pillai, S.C. Recent Advances in Photocatalysis for Environmental Applications. *J. Environ. Chem. Eng.* **2018**, *6*, 3531–3555. [[CrossRef](#)]
6. Mohamed, H.H.; Wazan, G.; Besisa, D.H.A. Natural Clay Minerals as Heterojunctions of Multi-Metal Oxides for Superior Photocatalytic Activity. *Mater. Sci. Eng. B* **2022**, *286*, 116077. [[CrossRef](#)]
7. Qian, W.; Hu, W.; Jiang, Z.; Wu, Y.; Li, Z.; Diao, Z.; Li, M. Degradation of Tetracycline Hydrochloride by a Novel CDs/g-C₃N₄/BiPO₄ under Visible-Light Irradiation: Reactivity and Mechanism Wei. *Catalysts* **2022**, *12*, 774. [[CrossRef](#)]

8. Lv, Y.; Gong, Z.; Ren, Z.; Guan, Y.; Wu, J.; Lv, K. Photocatalytic Degradation of Tetracycline Hydrochloride by Zinc oxide/Polypyrrole/Carbon nanotubes. *ChemistrySelect* **2023**, *8*, e202204762. [[CrossRef](#)]
9. Luu, T.V.H.; Nguyen, H.Y.X.; Nguyen, Q.T.; Nguyen, Q.B.; Nguyen, T.H.C.; Pham, N.C.; Nguyen, X.D.; Nguyen, T.K.; Dao, N.N. Enhanced Photocatalytic Performance of ZnO under Visible Light by Co-Doping of Ta and C Using Hydrothermal Method. *RSC Adv.* **2024**, *14*, 12954–12965. [[CrossRef](#)] [[PubMed](#)]
10. El Golli, A.; Contreras, S.; Dridi, C. Bio-Synthesized ZnO Nanoparticles and Sunlight-Driven Photocatalysis for Environmentally-Friendly and Sustainable Route of Synthetic Petroleum Refinery Wastewater Treatment. *Sci. Rep.* **2023**, *13*, 20809. [[CrossRef](#)] [[PubMed](#)]
11. Ahmad, I.; Bousbih, R.; Mahal, A.; Khan, W.Q.; Aljohani, M.; Jafar, N.N.; Jabir, M.S.; Majdi, H.; Alshomrany, A.S.; Shaban, M.; et al. Recent Progress in ZnO-Based Heterostructured Photocatalysts: A Review. *Mater. Sci. Semicond. Process.* **2024**, *180*, 108578. [[CrossRef](#)]
12. Cheng, F.; Liang, L.; Lin, G.; Xi, S. Enhanced Photoelectrocatalysis in Porous Single Crystalline Rutile Titanium Dioxide Electrodes. *J. Mater. Chem. A* **2024**, *12*, 3879–3885. [[CrossRef](#)]
13. Goutham, R.; Badri Narayan, R.; Srikanth, B.; Gopinath, K.P. *Supporting Materials for Immobilisation of Nano-Photocatalysts*; Springer: Berlin/Heidelberg, Germany, 2019; ISBN 9783030106096.
14. Elias, M.; Uddin, M.N.; Saha, J.K.; Hossain, M.A.; Sarker, D.R.; Akter, S.; Siddiquey, I.A.; Uddin, J. A Highly Efficient and Stable Photocatalyst; N-Doped ZnO/CNT Composite Thin Film Synthesized via Simple Sol-Gel Drop Coating Method. *Molecules* **2021**, *2*, 1470. [[CrossRef](#)] [[PubMed](#)]
15. Elias, M.; Amin, M.K.; Firoz, S.H.; Hossain, M.A.; Akter, S.; Hossain, M.A.; Uddin, M.N.; Siddiquey, I.A. Microwave-Assisted Synthesis of Ce-Doped ZnO/CNT Composite with Enhanced Photo-Catalytic Activity. *Ceram. Int.* **2017**, *43*, 84–91. [[CrossRef](#)]
16. AlMohamadi, H.; Awad, S.A.; Sharma, A.K.; Fayzullaev, N.; Távara-Aponte, A.; Chiguala-Contreras, L.; Amari, A.; Rodriguez-Benites, C.; Tphoon, M.A.; Esmaili, H.P. Photocatalytic Activity of Metal- and Non-Metal-Anchored ZnO and TiO₂ Nanocatalysts for Advanced Photocatalysis: Comparative Study. *Catalysts* **2024**, *14*, 420. [[CrossRef](#)]
17. Priyadharsan, A.; Ranjith, R.; Karmegam, N.; Thennarasu, G.; Ragupathy, S.; Oh, T.H.; Ramasundaram, S. Effect of Metal Doping and Non-Metal Loading on Light Energy Driven Degradation of Organic Dye Using ZnO Nanocatalysts. *Chemosphere* **2023**, *330*, 138708. [[CrossRef](#)] [[PubMed](#)]
18. Vallarasu, K.; Dinesh, S.; Nantha kumar, M.; Mithun, D.; Anitha, R.; Vijayalakshmi, V. ZnO Heterojunction Photocatalysts Prepared via Facile Green Synthesis Process Attaining Improved Photocatalytic Function for Degradation of Methylene Blue Dye. *Desalin. Water Treat.* **2024**, *318*, 100391. [[CrossRef](#)]
19. Chaudhary, D.; Singh, S.; Vankar, V.D.; Khare, N. ZnO Nanoparticles Decorated Multi-Walled Carbon Nanotubes for Enhanced Photocatalytic and Photoelectrochemical Water Splitting. *J. Photochem. Photobiol. A Chem.* **2018**, *351*, 154–161. [[CrossRef](#)]
20. Ossai, A.N.; Alabi, A.B.; Ezike, S.C.; Aina, A.O. Zinc Oxide-Based Dye-Sensitized Solar Cells Using Natural and Synthetic Sensitizers. *Curr. Res. Green Sustain. Chem.* **2020**, *3*, 100043. [[CrossRef](#)]
21. Wudil, Y.S.; Ahmad, U.F.; Gondal, M.A.; Al-Osta, M.A.; Almohammed, A.; Sa'ad, R.S.; Hrahsheh, F.; Haruna, K.; Mohamed, M.J.S. Tuning of Graphitic Carbon Nitride (g-C₃N₄) for Photocatalysis: A Critical Review. *Arab. J. Chem.* **2023**, *16*, 104542. [[CrossRef](#)]
22. Li, Y.; Yan, M.; Li, X.; Ma, J. Construction of Cu₂O-ZnO/Cellulose Composites for Enhancing the Photocatalytic Performance. *Catalysts* **2024**, *14*, 476. [[CrossRef](#)]
23. Lu, H.; Zhang, M.; Guo, M. Controllable Electrodeposition of ZnO Nanorod Arrays on Flexible Stainless Steel Mesh Substrate for Photocatalytic Degradation of Rhodamine B. *Appl. Surf. Sci.* **2014**, *317*, 672–681. [[CrossRef](#)]
24. Ko, Y.H.; Kim, M.S.; Yu, J.S. Structural and Optical Properties of ZnO Nanorods by Electrochemical Growth Using Multi-Walled Carbon Nanotube-composed Seed Layers. *Nanoscale Res. Lett.* **2012**, *7*, 1–6. [[CrossRef](#)] [[PubMed](#)]
25. Wei, Y.; Du, H.; Kong, J.; Lu, X.; Ke, L.; Sun, X.W. Multi-Walled Carbon Nanotubes Modified ZnO Nanorods: A Photoanode for Photoelectrochemical Cell. *Electrochim. Acta* **2014**, *143*, 188–195. [[CrossRef](#)]
26. Elias, M.; Uddin, M.N.; Hossain, M.A.; Saha, J.K.; Siddiquey, I.A.; Sarker, D.R.; Diba, Z.R.; Uddin, J.; Rashid Choudhury, M.H.; Firoz, S.H. An Experimental and Theoretical Study of the Effect of Ce Doping in ZnO/CNT Composite Thin Film with Enhanced Visible Light Photo-Catalysis. *Int. J. Hydrogen Energy* **2019**, *44*, 20068–20078. [[CrossRef](#)]
27. Desai, M.A.; Sharma, V.; Prasad, M.; Gund, G.; Jadkar, S.; Sartale, S.D. Photoelectrochemical Performance of MWCNT-Ag-ZnO Ternary Hybrid: A Study of Ag Loading and MWCNT Garnishing. *J. Mater. Sci.* **2021**, *56*, 8627–8642. [[CrossRef](#)]
28. Kuwajima, T.; Nakanishi, Y.; Yamamoto, A.; Nobusawa, K.; Ikeda, A.; Tomita, S.; Yanagi, H.; Ichinose, K.; Yoshida, T. Fabrication of Carbon Nanotube/Zinc Oxide Composite Films by Electrodeposition. *Jpn. J. Appl. Phys.* **2011**, *50*, 8–11. [[CrossRef](#)]
29. Hong, W.; Meng, M.; Liu, Q. Antibacterial and Photocatalytic Properties of Cu₂O/ZnO Composite Film Synthesized by Electrodeposition. *Res. Chem. Intermed.* **2017**, *43*, 2517–2528. [[CrossRef](#)]
30. Ren, P.; Deng, H.Y.; Zhang, J.X.; Dai, N. Nucleation Mechanism and Microstructural Analysis of Zn Films on Mo Substrates by Electrodeposition. *J. Electrochem. Soc.* **2016**, *163*, D309–D313. [[CrossRef](#)]

31. Kim, W.Y.; Kim, S.W.; Yoo, D.H.; Kim, E.J.; Hahn, S.H. Annealing Effect of ZnO Seed Layer on Enhancing Photocatalytic Activity of ZnO/TiO₂ Nanostructure. *Int. J. Photoenergy* **2013**, *2013*, 130541. [[CrossRef](#)]
32. Li, C.; Fang, G.; Li, J.; Ai, L.; Dong, B.; Zhao, X. Effect of Seed Layer on Structural Properties of ZnO Nanorod Arrays Grown by Vapor-Phase Transport Effect of Seed Layer on Structural Properties of ZnO Nanorod Arrays Grown by Vapor-Phase Transport. *J. Phys. Chem. C* **2008**, *112*, 990–995. [[CrossRef](#)]
33. Wang, S.F.; Tseng, T.Y.; Wang, Y.R.; Wang, C.Y.; Lu, H.C. Effect of ZnO Seed Layers on the Solution Chemical Growth of ZnO Nanorod Arrays. *Ceram. Int.* **2009**, *35*, 1255–1260. [[CrossRef](#)]
34. Ait hssi, A.; Atourki, L.; labchir, N.; Ouafi, M.; Abouabassi, K.; Elfanaoui, A.; Ihlal, A.; Bouabid, K. Electrodeposition of Oriented ZnO Nanorods by Two-Steps Potentiostatic Electrolysis: Effect of Seed Layer Time. *Solid State Sci.* **2020**, *104*, 106207. [[CrossRef](#)]
35. Wilson Balogun, S. Impact of Post-Deposition Heat Treatment on the Morphology and Optical Properties of Zinc Oxide (ZnO) Thin Film Prepared by Spin-Coating Technique. *J. Photonic Mater. Technol.* **2017**, *3*, 20. [[CrossRef](#)]
36. Cheol, W.; Pal, J.; Kim, Y.; Song, J.; Hwa, K.; Seong, T. Effect of Thermal Annealing on the Properties of ZnO Thin Films. *Vacuum* **2020**, *183*, 109776. [[CrossRef](#)]
37. Alshoaibi, A. The Influence of Annealing Temperature on the Microstructure and Electrical Properties of Sputtered ZnO Thin Films. *Inorganics* **2024**, *12*, 236. [[CrossRef](#)]
38. Haritha, A.H.; Cruz, M.E.; Sisman, O.; Duran, A.; Galusek, D.; Castro, Y.; Ceramics, O.; Cruz, M.E.; Sisman, O.; Duran, A.; et al. Influence of Annealing Temperature on the Photocatalytic Efficiency of Sol-Gel Dip-Coated ZnO Thin Films in Methyl Orange Degradation. *OPEN Ceram.* **2024**, *21*, 100727. [[CrossRef](#)]
39. Kang, F.; Sheng, G.; Yang, X.; Zhang, Y. Fabrication of Two-Dimensional Bi₂MoO₆ Nanosheet-Decorated Bi₂MoO₆/Bi₄O₅Br₂ Type II Heterojunction and the Enhanced Photocatalytic Degradation of Antibiotics. *Catalysts* **2024**, *12*, 289. [[CrossRef](#)]
40. Rayalu, S.S.; Mangrulkar, P.A.; Kamble, S.P.; Joshi, M.M.; Meshram, J.S.; Labhsetwar, N.K. Photocatalytic Degradation of Phenolics by N-Doped Mesoporous Titania under Solar Radiation. *Int. J. Photoenergy* **2012**, *2012*, 780562. [[CrossRef](#)]
41. Miceli, M.; Frontera, P.; Macario, A.; Malara, A. Recovery/Reuse of Heterogeneous Supported Spent Catalysts. *Catalysts* **2021**, *11*, 591. [[CrossRef](#)]
42. Habibi, M. Highly Impressive Activation of Persulfate Ions by Novel ZnO/CuCo O Nanostructures for Photocatalytic Removal of Tetracycline Hydrochloride under Visible Light. *Environ. Technol. Innov.* **2021**, *24*, 102038. [[CrossRef](#)]
43. Liu, D.; Li, H.; Gao, R.; Zhao, Q.; Yang, Z.; Gao, X.; Wang, Z.; Zhang, F.; Wu, W. Enhanced Visible Light Photoelectrocatalytic Degradation of Tetracycline Hydrochloride by I and P Co-Doped TiO₂ Photoelectrode. *J. Hazard. Mater.* **2021**, *406*, 124309. [[CrossRef](#)] [[PubMed](#)]
44. Liu, J.; Zhang, S.; Wang, W.; Zhang, H. Photoelectrocatalytic Principles for Meaningfully Studying Photocatalyst Properties and Photocatalysis Processes: From Fundamental Theory to Environmental Applications. *J. Energy Chem.* **2023**, *86*, 84–117. [[CrossRef](#)]
45. Pedanekar, R.S.; Mohite, S.V.; Madake, S.B.; Kim, Y.; Gunjekar, J.L.; Rajpure, K.Y. Photoelectrocatalytic Activity of Methylene Blue Using Chemically Sprayed Bi₂WO₆ Photoanode under Natural Sunlight. *J. Alloys Compd.* **2023**, *942*, 168866. [[CrossRef](#)]
46. Suhadolnik, L.; Pohar, A.; Likozar, B.; Čeh, M. Mechanism and Kinetics of Phenol Photocatalytic, Electrocatalytic and Photoelectrocatalytic Degradation in a TiO₂-Nanotube Fixed-Bed Microreactor. *Chem. Eng. J.* **2016**, *303*, 292–301. [[CrossRef](#)]
47. Torres-Pinto, A.; Díez, A.M.; Silva, C.G.; Faria, J.L.; Sanromán, M.Á.; Silva, A.M.T.; Pazos, M. Photoelectrocatalytic Degradation of Pharmaceuticals Promoted by a Metal-Free G-C₃N₄ Catalyst. *Chem. Eng. J.* **2023**, *476*, 146761. [[CrossRef](#)]
48. Li, T.; Wang, Z.; Liu, C.; Tang, C.; Wang, X.; Ding, G.; Ding, Y.; Yang, L. TiO₂ Nanotubes/Ag/MoS₂ Meshy Photoelectrode with Excellent Photoelectrocatalytic Degradation Activity for Tetracycline Hydrochloride. *Nanomaterials* **2018**, *8*, 666. [[CrossRef](#)] [[PubMed](#)]
49. Slimi, B.; Ben Assaker, I.; Kriaa, A.; Marí, B.; Chtourou, R. One-Step Electrodeposition of Ag-Decorated ZnO Nanowires. *J. Solid State Electrochem.* **2017**, *21*, 1253–1261. [[CrossRef](#)]
50. Hezam, F.A.; Nur, O.; Mustafa, M.A. Synthesis, Structural, Optical and Magnetic Properties of NiFe₂O₄/MWCNTs/ZnO Hybrid Nanocomposite for Solar Radiation Driven Photocatalytic Degradation and Magnetic Separation. *Colloids Surfaces A Physicochem. Eng. Asp.* **2020**, *592*, 124586. [[CrossRef](#)]
51. Wang, M.; Zhou, Y.; Zhang, Y.; Hahn, S.H.; Kim, E.J. From Zn(OH)₂ to ZnO: A Study on the Mechanism of Phase Transformation. *CrystEngComm* **2011**, *13*, 6024–6026. [[CrossRef](#)]
52. Bui, Q.C.; Salem, B.; Roussel, H.; Mescot, X.; Guerfi, Y.; Jiménez, C.; Consonni, V.; Ardila, G. Effects of Thermal Annealing on the Structural and Electrical Properties of ZnO Thin Films for Boosting Their Piezoelectric Response. *J. Alloys Compd.* **2021**, *870*, 159512. [[CrossRef](#)]
53. Ahmed, N.M.; Sabah, F.A.; Abdulgafour, H.I.; Alsadig, A.; Sulieman, A.; Alkhoaryef, M. The Effect of Post Annealing Temperature on Grain Size of Indium-Tin-Oxide for Optical and Electrical Properties Improvement. *Results Phys.* **2019**, *13*, 102159. [[CrossRef](#)]
54. Kabir, M.H.; Ali, M.M.; Kaiyum, M.A.; Rahman, M.S. Effect of Annealing Temperature on Structural Morphological and Optical Properties of Spray Pyrolyzed Al-Doped ZnO Thin Films. *J. Phys. Commun.* **2019**, *3*, 105007. [[CrossRef](#)]

55. Soonmin, H. Investigation of Optical Properties of Thin Films by Means of UV-Visible Spectrophotometer: A Review. *New Front. Phys. Sci. Res.* **2022**, *5*, 66–82. [[CrossRef](#)]
56. Baishya, K.; Ray, J.S.; Dutta, P.; Das, P.P.; Das, S.K. Graphene-Mediated Band Gap Engineering of WO₃ Nanoparticle and a Relook at Tauc Equation for Band Gap Evaluation. *Appl. Phys. A Mater. Sci. Process.* **2018**, *124*, 704. [[CrossRef](#)]
57. Sabeeh, S.H.; Jassam, R.H. The Effect of Annealing Temperature and Al Dopant on Characterization of ZnO Thin Films Prepared by Sol-Gel Method. *Results Phys.* **2018**, *10*, 212–216. [[CrossRef](#)]
58. Caglar, M.; Ilican, S.; Caglar, Y.; Yakuphanoglu, F. Electrical Conductivity and Optical Properties of ZnO Nanostructured Thin Film. *Appl. Surf. Sci.* **2009**, *255*, 4491–4496. [[CrossRef](#)]
59. Wang, Y.; Tang, W.; Zhang, L.; Zhao, J. Electron Concentration Dependence of Optical Band Gap Shift in Ga-Doped ZnO Thin Films by Magnetron Sputtering. *Thin Solid Films* **2014**, *565*, 62–68. [[CrossRef](#)]
60. Hung-Chun Lai, H.; Basheer, T.; Kuznetsov, V.L.; Egdell, R.G.; Jacobs, R.M.J.; Pepper, M.; Edwards, P.P. Dopant-Induced Bandgap Shift in Al-Doped ZnO Thin Films Prepared by Spray Pyrolysis. *J. Appl. Phys.* **2012**, *112*, 83708. [[CrossRef](#)]
61. Dac Dien, N. Preparation of Various Morphologies of ZnO Nanostructure through Wet Chemical Methods. *Adv. Mater. Sci.* **2019**, *4*, 1–5. [[CrossRef](#)]
62. Abdel-Fattah, T.M.; Wixtrom, A.; Zhang, K.; Cao, W.; Baumgart, H. Highly Uniform Self-Assembled Gold Nanoparticles over High Surface Area ZnO Nanorods as Catalysts. *ECS J. Solid State Sci. Technol.* **2014**, *3*, M61–M64. [[CrossRef](#)]
63. Clabel, H.J.L.; Awan, I.T.; Rivera, V.A.G.; Nogueira, I.C.; Pereira-da-Silva, M.A.; Li, M.S.; Ferreira, S.O.; Marega, E. Growth Process and Grain Boundary Defects in Er Doped BaTiO₃ Processed by EB-PVD: A Study by XRD, FTIR, SEM and AFM. *Appl. Surf. Sci.* **2019**, *493*, 982–993. [[CrossRef](#)]
64. Lv, J.; Gong, W.; Huang, K.; Zhu, J.; Meng, F.; Song, X.; Sun, Z. Effect of Annealing Temperature on Photocatalytic Activity of ZnO Thin Films Prepared by Sol-Gel Method. *Superlattices Microstruct.* **2011**, *50*, 98–106. [[CrossRef](#)]
65. Chen, C.S.; Xie, X.D.; Cao, S.Y.; Liu, T.G.; Lin, L.W.; Chen, X.H.; Liu, Q.C.; Kuang, J.C.; Xiao, Y. Preparation and Photocatalytic Activity of Multi-Walled Carbon Nanotubes/Mg-Doped ZnO Nanohybrids. *Mater. Sci. Pol.* **2015**, *33*, 460–469. [[CrossRef](#)]
66. López Guemez, A.d.R.; Cordero García, A.; Cervantes López, J.L.; Pérez Vidal, H.; Díaz Flores, L.L. Evaluation of the Photocatalytic Activity of ZnO Nanorods and Nanoflowers Grown from Seed Layers Deposited by Spin Coating. *Bol. La Soc. Esp. Ceram. Y Vidr.* **2023**, *63*, 72–84. [[CrossRef](#)]
67. Ikizler, B.; Peker, S.M. Effect of the Seed Layer Thickness on the Stability of ZnO Nanorod Arrays. *Thin Solid Films* **2014**, *558*, 149–159. [[CrossRef](#)]
68. Song, C.; Liu, H.Y.; Guo, S.; Wang, S.G. Photolysis Mechanisms of Tetracycline under UV Irradiation in Simulated Aquatic Environment Surrounding Limestone. *Chemosphere* **2020**, *244*, 125582. [[CrossRef](#)]
69. Ait hssi, A.; Amaterz, E.; labchir, N.; Atourki, L.; Bouderbala, I.Y.; Elfanaoui, A.; Benlhachemi, A.; Ihlal, A.; Bouabid, K. Electrodeposited ZnO Nanorods as Efficient Photoanodes for the Degradation of Rhodamine B. *Phys. Status Solidi Appl. Mater. Sci.* **2020**, *217*, 2000349. [[CrossRef](#)]
70. Gan, W.Y.; Friedmann, D.; Amal, R.; Zhang, S.; Chiang, K.; Zhao, H. A Comparative Study between Photocatalytic and Photoelectrocatalytic Properties of Pt Deposited TiO₂ Thin Films for Glucose Degradation. *Chem. Eng. J.* **2010**, *158*, 482–488. [[CrossRef](#)]
71. Rokade, A.; Rondiya, S.; Gabhale, B.; Diwate, K.; Karpe, S.; Mayabadi, A.; Pandharkar, S.; Sharma, V.; Lonkar, G.; Pathan, H.; et al. Electrodeposition of Template Free Hierarchical ZnO Nanorod Arrays via a Chloride Medium. *J. Mater. Sci. Mater. Electron.* **2016**, *27*, 12357–12364. [[CrossRef](#)]

Disclaimer/Publisher's Note: The statements, opinions and data contained in all publications are solely those of the individual author(s) and contributor(s) and not of MDPI and/or the editor(s). MDPI and/or the editor(s) disclaim responsibility for any injury to people or property resulting from any ideas, methods, instructions or products referred to in the content.